◎ 논 문

# LARGE EDDY SIMULATION OF THE COMPRESSIBLE FLOW OVER A CAVITY WITH HIGH ASPECT RATIO

Keon Je Oh*

Large eddy simulation is used to investigate the compressible flow over a cavity with high aspect ratio. The sub-grid scale stresses are modeled using the dynamic model. The compressible Navier-Stokes equations are solved with the sixth order accurate compact finite difference scheme in the space and the 4th order Runge-Kutta scheme in the time. The buffer zone techniques are used for non-reflecting boundary conditions. The results show the shear layer oscillation over the cavity. The votical disturbances, the roll-up of vorticity, and impingement and scattering of vorticity at the downstream cavity edge can be seen in the shear layer. Several peaks for the resonant frequencies are found in the spectra of the vertical velocity at the center-line. The most energetic peak near the downstream edge is different from that at the center part of the cavity. The pressure has its minimum value in the vortex core inside the cavity, and becomes very high at the downstream face of the cavity. The variation of the model coefficient predicted by the dynamic model is quite large between 0 and 0.3. The model coefficient increases in the stream-wise evolution of the shear layer and sharply decreases near the wall due to the wall effect.

**Key Words**: Cavity Flow, Compressible Flow, LES, Dynamic Model

## 1. Introduction

It is of a great practical importance to study the flows over the open cavity. The acoustic noise emits by the flow over the cavity. The emission of the noise is due to the resonant oscillations in the flow. Cavity resonance is thought to arise from a feedback loop in the flow over the cavity; shear layer instability, the impingement of the vortices at the downstream edge, the transmission of acoustic waves upstream, and their conversion to votical fluctuations at the cavity leading edge. This feedback process is first investigated by Rossiter[1]. His semi-empirical formula to predict the resonant frequencies is widely used. The resonance phenomena over the cavity are influenced by the turbulence in the flow. The spreading is more rapid by the generation of Reynolds stresses and other nonlinear interactions in the turbulence. The amplification of disturbances is attenuated by the dissipation mechanism in turbulent flows. The resonance phenomenon in turbulent flows is very complex and a full modeling of the process is impossible. Numerical simulations of the compressible flow over the cavity can give better understanding of the resonance phenomenon.

* 2003년 7월 21일 접수

*정회원, Department of Mechanical Engineering, Kyungnam University, Masan 631-701, Korea

Recently, Colonius et al.[2] provided 2-dimensional DNS (Direct Numerical Simulation) results on the cavity flow. They assumed that the resonant modes are two-dimensional and tried DNS for unstable laminar flows without any turbulence model.

Their results showed an interesting transition from a shear layer mode of oscillation to a wake mode of oscillation. The results from the computation were in good agreement with experimental data. The acoustic field was well represented by the DNS simulations. However, this case is only for the two-dimensional flow and cannot be applied to turbulent and three dimensional cavity flows. DNS of the 3-dimensional cavity flow is limited to low Reynolds number and would be quite expensive because it needs much computing time. Another simulation technique of turbulent flows is the LES (Large Eddy Simulation). The large scale is resolved in the computation while the small scales are modeled with a simple model. LES is based on the fact that the small scales are not important and they do not contain much energy. LES has a great advantage that it can be applied to a high Reynolds number flow and it can simulate the unsteady turbulent flow with less computing time than DNS.

The author investigated the compressible flow over a cavity using large eddy simulation[3,4]. The results showed a typical shear layer oscillation of the cavity flow. In the present study, the LES method is used to calculate the compressible flows over an open and somewhat long cavity with high aspect ratio. The dynamic model is used for modeling the sub-grid scale stresses. The resonant frequencies over the cavity are predicted from the calculation and compared with those of the empirical relation. The time dependent flow field and mean flow quantities are investigated inside and over the cavity.

## 2. Governing equations

The governing equations for compressible flows over the cavity as shown in Fig. 1 are the continuity, momentum, and energy equations given by

$$\frac{\partial \rho}{\partial t} + \frac{\partial \rho u_i}{\partial x_i} = 0 \tag{1}$$

$$\frac{\partial \rho u_i}{\partial t} + \frac{\partial \rho u_i u_j}{\partial x_j} = -\frac{\partial p}{\partial x_i} + \frac{\partial \sigma_{ij}}{\partial x_j} \tag{2}$$

$$\frac{\partial \rho E}{\partial t} + \frac{\partial (\rho E + p) u_j}{\partial x_j} = \frac{\partial}{\partial x_j}(k \frac{\partial T}{\partial x_j}) + \frac{\partial u_i \sigma_{ij}}{\partial x_j} \tag{3}$$

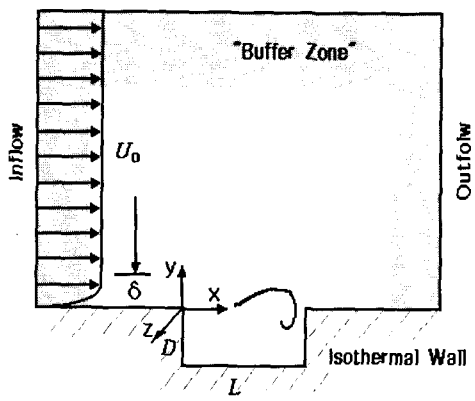


**Fig. 1** Schematic diagram of cavity configuration and computational domain

where $\sigma_{ij}$ is the Newtonian stress tensor, $E$ is the total energy per unit mass(internal and kinetic), $p$ is the pressure, and $T$ is the temperature:

$$\sigma_{ij} = \mu(\frac{\partial u_i}{\partial x_j} + \frac{\partial u_j}{\partial x_i} - \frac{2}{3}\delta_{ij}\frac{\partial u_k}{\partial x_k}) \tag{4}$$

$$\rho E = \rho e + \frac{1}{2}\rho u_i u_i \tag{5}$$

$$p = (\gamma - 1)\rho e \tag{6}$$

$$T = \frac{\gamma}{\rho C_P}(\rho e) \tag{7}$$

The flow variables are filtered in the space for large eddy simulations.

$$\bar{f}(x_1, x_2, x_3) = \int_{x_1'}\int_{x_2'}\int_{x_3'} \prod_{i=1}^{3} G_i(x_i; x_i')\, f(x_1', x_2', x_3')\, dx_1' dx_2' dx_3' \tag{8}$$

$G_i$ is a spatial filter which is chosen as the top hat filter in the present study.

$$G_i(x_i : x_i') = 1/\Delta_i \quad if \ |x_i - x_i'| \le \Delta_i/2$$
$$= 0 \qquad otherwise \tag{9}$$

$\Delta_i$ is the filter width in the i-th direction. A Favre filtered variable for compressible flows is defined as

$$\tilde{f} = \frac{\overline{\rho f}}{\bar{\rho}} \tag{10}$$

The Favre filtered governing equations are given by

$$\frac{\partial \bar{\rho}}{\partial t} + \frac{\partial \overline{\rho u_i}}{\partial x_i} = 0 \tag{11}$$

$$\frac{\partial \overline{\rho u_i}}{\partial t} + \frac{\partial \overline{\rho u_i \tilde{u}_j}}{\partial x_j} = -\frac{\partial \bar{p}}{\partial x_i} + \frac{\partial \bar{\sigma}_{ij}}{\partial x_j} - \frac{\partial}{\partial x_j}(\overline{\rho u_i u_j} - \overline{\rho u_i}\tilde{u}_j) \tag{12}$$

$$\frac{\partial \overline{\rho E}}{\partial t} + \frac{\partial (\overline{\rho E} + \bar{P})\tilde{u}_j}{\partial x_j} = \frac{\partial}{\partial x_j}(k\frac{\partial \bar{T}}{\partial x_j}) + \frac{\partial \bar{u}_i \bar{\sigma}_{ij}}{\partial x_j} - \frac{\partial}{\partial x_j}\{(\overline{\rho E} + \bar{P})\tilde{u}_j - (\overline{\rho E} + \bar{P})\tilde{u}_j\} \tag{13}$$

$$\bar{p} = (\gamma - 1)[\overline{\rho E} - \frac{1}{2}\overline{\rho u_i u_i}] \tag{14}$$

$$\tilde{T} = \frac{\gamma}{\bar{\rho} C_P}(\overline{\rho E} - \frac{1}{2}\overline{\rho u_i u_i}) \tag{15}$$

The sub-grid scale stress tensor can be denoted by $\tau_{ij}$, and the sub-grid scale term in the energy equation can be rewritten with the sub-grid scale heat flux as described below.

$$\tau_{ij} = (\overline{\rho u_i u_j} - \overline{\rho}\tilde{u}_i\tilde{u}_j) \tag{16}$$

$$\overline{(\rho E + p)u_j} - (\overline{\rho E} + \bar{p})\tilde{u}_j = \{\overline{(\rho e + p)u_j} - (\overline{\rho e} + \bar{p})\tilde{u}_j\} + \{\overline{\frac{1}{2}\rho u_i u_i u_j} - \overline{\frac{1}{2}\rho u_i u_i}\tilde{u}_j\} \tag{17}$$

$$Q_j = \overline{(\rho e + p)u_j} - (\overline{\rho e} + \bar{p})\tilde{u}_j = \overline{\rho h u_j} - \bar{\rho}\tilde{h}\tilde{u}_j = \overline{\rho C_P T u_j} - \bar{\rho} C_P \tilde{T}\tilde{u}_j \tag{18}$$

The last term in the equation (17) can be approximated by[5]

$$\overline{\frac{1}{2}\rho u_i u_i u_j} - \overline{\frac{1}{2}\rho u_i u_i}\tilde{u}_j = \overline{\rho K u_j} - \bar{\rho}\tilde{K}\tilde{u}_j = \tau_{ij}\tilde{u}_i \tag{19}$$

Also, the sub-grid scale contributions in the viscous terms, non-linearities in the heat fluxes, and the sub-grid contributions in the kinetic energy are expected to be small and the followings are assumed.

$$\frac{\partial \bar{\sigma}_{ij}}{\partial x_j}=\frac{\partial \tilde{\sigma}_{ij}}{\partial x_j} \quad , \quad \frac{\partial \overline{u_i \sigma_{ij}}}{\partial x_j}=\frac{\partial \tilde{u}_i \tilde{\sigma}_{ij}}{\partial x_j}$$
$$k\frac{\partial \bar{T}}{\partial x_j}=k\frac{\partial \tilde{T}}{\partial x_j} \quad , \quad \frac{1}{2}\overline{\rho u_i u_i}=\frac{1}{2}\bar{\rho}\tilde{u}_i\tilde{u}_j \qquad (20)$$

The sub-grid scale stresses and heat flux can be expressed by the eddy viscosity model

$$\tau_{ij}-\frac{1}{3}\tau_{kk}\delta_{ij}=-2\bar{\rho}\nu_t(\tilde{S}_{ij}-\frac{1}{3}\tilde{S}_{kk}\delta_{ij}) \qquad (21)$$

$$Q_j=-\frac{\bar{\rho}\nu_t C_P}{\mathrm{Pr}_t}\frac{\partial \tilde{T}}{\partial x_j} \qquad (22)$$

where $\tilde{S}_{ij}$ is the Favred filtered strain rate tensor,

$$\tilde{S}_{ij}=\frac{1}{2}(\frac{\partial \tilde{u}_i}{\partial x_j}+\frac{\partial \tilde{u}_j}{\partial x_i}) \qquad (23)$$

and $\mathrm{Pr}_t$ is the turbulent Prandtl number which is taken as 0.9[6].The isotropic part of the sub-grid scale stress tensor $\tau_{kk}$ is assumed to be small and neglected in the present study. The eddy viscosity is given by the sub-grid scale characteristics length and velocity:

$$\nu_t=C^2\Delta^2(2\tilde{S}_{ij}\tilde{S}_{ij})^{1/2} \qquad (24)$$

where $\Delta$ is defined as $\Delta^2=(\Delta_1\Delta_2\Delta_3)^{2/3}$. The model constant C is fixed during the calculation in the Smagorinsky model. The Smagorinsky constant is known to have a value between 0.1 and 0.24[6].

The weakness of the Smagorinsky model is that the model coefficient must be given by the optimization in computation and the optimal value cannot be general for the turbulent flows. Germano et al.[7] proposed a sub-grid scale model to overcome this deficiency. They developed the concept to determine the model coefficient using the filtering of the flow variable at two different scales. In this model, the model coefficient C is "dynamically" determined in the space and in the time by the resolved flow variables. Moin et al.[8] extend this concept to the compressible flow. We use the dynamic model for $\tau_{ij}$. The sub-grid scale stress $\tau_{ij}$ is written as:

$$\tau_{ij}=\overline{\rho u_i u_j}-\bar{\rho}\tilde{u}_i\tilde{u}_j=\overline{\rho u_i u_j}-\frac{\overline{\rho u_i}\,\overline{\rho u_j}}{\bar{\rho}} \qquad (25)$$

The dynamic model uses a test filter with a larger filter width $(=k\Delta)$ than the grid filter $(k>1)$. The ratio of the two filter widths is chosen as 2[7]. The consecutive application of these two filters yields the test-filtered stresses :

$$\tau_{ij}^{*}=\overline{\overline{\rho u_i u_j}}-\frac{\overline{\overline{\rho u_i}}\,\overline{\overline{\rho u_j}}}{\overline{\overline{\rho}}}=\overline{\overline{\rho u_i u_j}}-\frac{\overline{\overline{\rho}\tilde{u}_i}\,\overline{\overline{\rho}\tilde{u}_j}}{\overline{\overline{\rho}}} \qquad (26)$$

The Leonard stresses $L_{ij}$ can be expressed in terms of $L_{ij}$ and $\tau_{ij}^{*}$.

$$L_{ij}=\tau_{ij}^{*}-\overline{\tau_{ij}}=\overline{\bar{\rho}\tilde{u}_i\tilde{u}_j}-\frac{\overline{\bar{\rho}\tilde{u}_i}\,\overline{\bar{\rho}\tilde{u}_j}}{\overline{\bar{\rho}}} \qquad (27)$$

The test-filtered sub-grid scale stresses can be modeled using the Smagorinsky model with the same model coefficient and the test filtered variables.

$$\tau_{ij}^{*}-\frac{1}{3}\tau_{kk}^{*}=-2C^2\overline{\bar{\rho}}(k\Delta)^2|\overline{\tilde{S}_{ij}}|(\overline{\tilde{S}_{ij}}-\frac{1}{3}\overline{\tilde{S}_{kk}}\delta_{ij}) \qquad (28)$$

The sub-grid scale stresses are directly filtered using the test filter as follows.

$$\overline{\tau_{ij}} - \frac{1}{3}\overline{\tau_{kk}}\delta_{ij} = -2C^2\overline{\rho}\overline{\Delta^2}\,|\widetilde{S}_{ij}|(\widetilde{S}_{ij} - \frac{1}{3}\widetilde{S}_{kk}\delta_{ij}) \quad (29)$$

Combining Eq. (27)-(29) yields

$$L_{ij} - \frac{1}{3}L_{kk}\delta_{ij} = -2C^2 M_{ij} \quad (30)$$

with

$$L_{ij} = \overline{\overline{\rho}\widetilde{u}_i\widetilde{u}_j} - \frac{\overline{\overline{\rho}\widetilde{u}_i}\;\overline{\overline{\rho}\widetilde{u}_j}}{\overline{\overline{\rho}}} \quad (31)$$

$$M_{ij} = \overline{\overline{\rho}(k\Delta)^2\,|\widetilde{S}_{ij}|(\widetilde{S}_{ij} - \frac{1}{3}\widetilde{S}_{kk}\delta_{ij})} - \overline{\overline{\rho}\Delta^2\,|\widetilde{S}_{ij}|(\widetilde{S}_{ij} - \frac{1}{3}\widetilde{S}_{kk}\delta_{ij})} \quad (32)$$

We can use this relation to determine $C$ since all terms except $C$ can be computed from the resolved variables. Another procedure is needed to obtain $C$ because there are six equations to be solved for one constant $C$. The least square error method is employed to calculate $C$ in the present study[9], and $C$ can be determined as

$$C^2 = -\frac{1}{2}\frac{L_{ij}M_{ij}}{M_{ij}M_{ij}} \quad (33)$$

The numerator and denominator of the equation need volume averaging in the space because they can become zero at some grid points. In the present calculation, the numerator and the denominator of the equation are averaged in the z-direction.

## 3. Numerical method and boundary conditions

The numerical method is very similar to the methods used by Colonius et al.[2]. The compressible Navier-Stokes equations are solved with the sixth order accurate compact finite difference scheme[10] in the space and the 4th order Runge-Kutta scheme in the time. To minimize the aliasing error, the convection terms are rewritten in the skew symmetric form[11], i.e.,

$$\frac{\partial\overline{\rho}\widetilde{u}_i\widetilde{u}_j}{\partial x_j} = \frac{1}{2}\left(\frac{\partial\overline{\rho}\widetilde{u}_i\widetilde{u}_j}{\partial x_j} + \widetilde{u}_i\frac{\partial\overline{\rho}\widetilde{u}_j}{\partial x_j} + \overline{\rho}\widetilde{u}_j\frac{\partial\widetilde{u}_i}{\partial x_j}\right) \quad (34)$$

At inflow, outflow, and normal boundaries, the one dimensional boundary conditions of Poinsot and Lele[12] are used and the buffer regions with artificial damping terms are placed[13]. In the buffer zone, the numerical solutions are forced to a certain target solution and the acoustic wave is allowed to pass freely with minimal reflection. At the wall, non-slip conditions for the velocity and isothermal condition for the temperature are enforced. A periodic boundary condition is used in the span-wise direction.

## 4. Calculation

The origin of the coordinate system is located at the upstream corner of the cavity as shown in Fig. 1. The inflow is located at $x/D$=-5.406 ($D$: cavity depth) upstream of the cavity and the outflow is located at $x/D$=16.945 downstream of the cavity. The vertical extent of the domain is *6.98D* over the cavity. Computational domain includes the buffer zone of *1.25D*, *2.0D*, and *2.0D* at the inflow, outflow, and normal boundary, respectively. Calculations are performed on a grid system with two blocks. The number of

grid point is (418, 95, 30) over the cavity and (180, 35, 30) inside the cavity in the x, y, and z direction, respectively. The grid is clustered near all the walls. Analytical error function mappings are used for the grid clustering. The initial velocity profiles on the wall and over the cavity are given by the Blasius boundary layer solutions. No initial motion is assumed inside the cavity. To initiate three dimensional turbulent flow motions, a uniform random perturbation is added to the span-wise velocity at all grid points.

The equations are made to be dimensionless with the cavity depth(D), ambient speed of sound($C_o$), and ambient density. The following parameters may be independent variables in the simulations: the cavity length and width relative to the cavity depth (L/D, W/D), the initial boundary layer thickness at the cavity leading edge relative to the cavity depth ($\delta$/D), the Mach number of the free stream ($M=U_\infty/C_o$), and the Reynolds number based on the ambient speed of sound and the cavity depth (Re). Calculation is made for the case of L/D=8, W/D=8.0, $\delta$/D=0.2967, M=0.6, Re=1500. The Reynolds number is low in the present calculation for numerical stability because we use high order numerical scheme. Calculation is started with randomly perturbed initial velocity field. The time increment is chosen as $\Delta t \cdot C_\infty/D=0.0079$ and the calculation is advanced up to 16000 time steps.

Fig. 2 shows the time traces of the normal velocity averaged in the span-wise direction at $y$=0. The figure confirms the oscillatory motion over the cavity. The velocity variations are quite large in the latter part of the cavity. Oscillatory motion feature at x/L=0.9 is different from those at other two locations. This indicates that the flow around the downstream corner of the cavity becomes more complex by impingement of the shear layer.

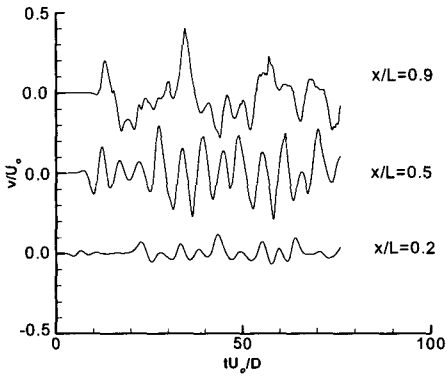


**Fig. 2** Time traces of the normal velocity averaged in the spanwise direction at $y$=0.

To investigate the oscillatory motion in detail, the instantaneous vorticity contours averaged in the span-wise direction are shown at different times in Fig. 3. Colonius et al.[2] showed that there are two types of flow mode over the cavity, i.e., the shear layer mode and the wake mode. The shear layer mode is characterized by the feedback process described in the introduction. The wake mode is characterized instead by a large-scale vortex shedding inside the cavity.

Fig. 3 shows a typical flow pattern of the shear layer mode of oscillation. The votical disturbances are clear in the shear layer along the center line ($y$=0) over the cavity. The roll-up of vorticity in the shear layer and impingement and scattering at the downstream cavity edge can be seen. The flow inside cavity is nearly same at different times and does not show a large-scale vortex shedding which implies the wake mode. The steadiness of the vortex in the cavity indicates that the interaction of the flow inside the cavity with the shear layer is not much.

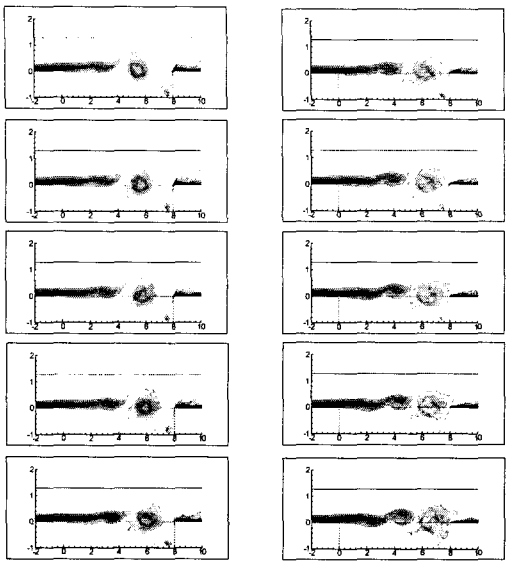

**Fig. 3** Instantaneous vorticity contours averaged in the spanwise direction at different times.

Fig.4 shows the spectrum of normal velocity at the center-line(y=0) for the two different locations, x/L=0.5 and 0.9. As shown in Fig.3, roll-up of the vorticity appears around x/L=0.5 and the vorticity eddies interacts with the downstream corner of the cavity with impingement and scattering around x/L=0.9. Similar distinct peaks can be seen in the spectra, but the most energetic peaks are different between x/L=0.5 and 0.9. The primary peak is found at 0.718 for x/L=0.5, while it is found at 0.154 for x/L=0.9. This indicates that the flow around the downstrean corner is dominated by a lower frequency which comes from the flow interaction with the wall of the cavity. In the previous calculations for a cavity with L/D=4[3,4], the results showed that only one peak appeared in the spectrum and the peak value was not different between the center and latter part of the cavity. This indicates that the flow oscillation over the long cavity becomes more complex by the flow interaction around the downstream edge of the cavity. The flow oscillations over the rectangular cavity show discrete frequencies by cavity resonance. Cavity resonance is thought to arise from the coupling between shear layer instability and acoustic feedback[1,14]. Rossiter [1] presented the following formula to predict the resonant frequencies for compressible flows over the cavity.

$$St_n = \frac{f_n L}{U_0} = \frac{n-\alpha}{M+\frac{1}{k}}, \quad n = 1, 2, . \tag{35}$$

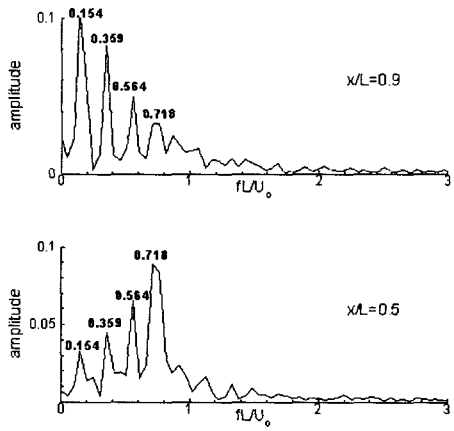


**Fig. 4** Spectra of the normal velocity averaged in the spanwise direction at $y$=0.

where $St_n$ is the Strouhal number corresponding to the n-th mode frequency $f_n$, L is the cavity length, $U_o$ is the free stream velocity, M is the Mach number, k is the average phase speed of the votical disturbances, and $\alpha$ is an empirical constant. $k$ and $\alpha$ are taken as 0.57 and 0.25, respectively [1,14]. In Fig. 4, distinct peaks in the spectra can be compared with the predictions from the Rossiter formula. Two peaks in the spetra can be detected around the first and the second mode of the Rossiter formula, i.e., $St_1 = 0.319$ and $St_2 = 0.74$.

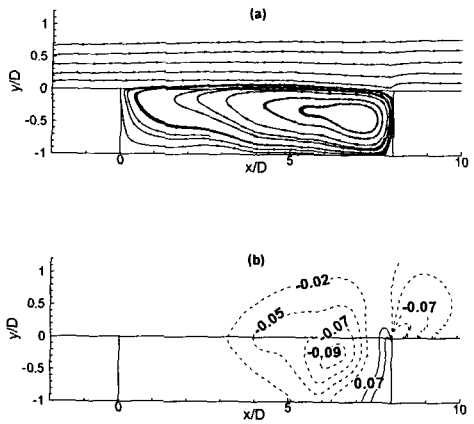


**Fig. 5** Time averaged mean streamlines and the pressure coefficient contours ((a)streamlines, (b)pressure coefficient (dashed negative values))

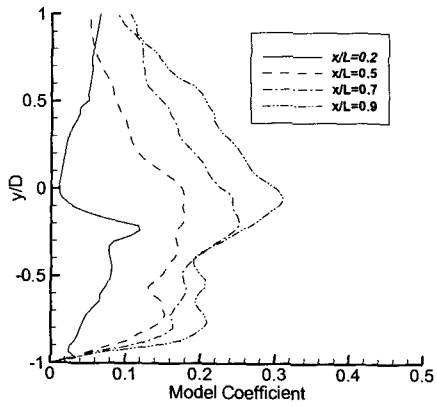


**Fig. 6** Time averaged model coefficient distributions at different streamwise positions.

Fig. 5 shows the time averaged mean streamlines and the pressure coefficient distribution. The mean flow streamlines in the shear layer over the cavity are nearly horizontal along the mouth of the cavity. Flow re-circulation is induced inside the cavity. There is a strong stationary vortex within the cavity, which is centered in the latter part of the cavity. The pressure coefficient variation is not quite large except in the region of the latter part of the cavity. The pressure becomes very low in the center of the re-circulation region. The low pressure is due to the vortical swirling motion. It is noted that the pressure is very high at the downstream face of the cavity. A sudden increase of the pressure is associated with the impingement and interaction of the vortices with the dowastream wall of the cavity. In the cavity flow calculations for L/D=4[3,4], the pressure on the downstream face was not so high, and it can be seen that the flow interaction at the downstream corner becomes more strong for the present case of L/D=8.

We investigate the variation of the time averaged model coefficient at several stream-wise locations in Fig. 6. It is noted that the coefficient is known as 0.1-0.24 in the Smagorinsky model. The variation of the model coefficient predicted by the dynamic model is quite large between 0 and 0.3. These results point to a deficiency of the Smagorinsky model with a fixed coefficient. The model coefficient increases in the stream-wise evolution of the shear layer and becomes larger in the latter part of the cavity. However, the value of the model coefficient appears to be independent of the stream-wise location in the free stream over the shear layer. The model coefficient sharply decreases near the wall due to the wall effect.

## 5. Conclusions

In the present study, the LES method with the dynamic model is applied to calculate the compressible flow over an open and long cavity. The results can show the characteristics of the shear layer oscillation over the cavity. The spectra of the vertical velocity at the center-line show several distinct peaks for the resonant frequencies.

The most energetic peak near the downstream edge is different from that at the center part. Two peaks in the spetra can be detected around the first and the second mode of the Rossiter formula. The pressure has its minimum value in the center of the re-circulation region. A sharp increase of the pressure is seen at the downstream face, which is due to the flow interaction with the downstream wall. The value of the model coefficient varies quite large between 0.0 and 0.3. This indicates a deficiency of the Smagorinsky model with a fixed model coefficient.

## Acknowledgments

This research was supported by the 2003 Kyungnam university research fund. Also, I would like to thank Prof. Colonius at CALTECH for his advice in conducting this research.

## References

[1] Rossiter, J.E., "Wind tunnel experiments on the flow over rectangular cavities at subsonic and transonic speeds", Technical Report 3438, Aeronautical Research Council Reports and Memoranda.(1964).

[2] Colonius, T., Basu, A. J., and Rowley., C.W., "Numerical investigation of the flow past a cavity", AIAA (1999), pp.99-1912.

[3] Oh, K., and Colonius, T., "Large eddy simulation of the compressible flow over an open cavity", Proceedings of the ASME Fluids engineering summer meeting, FEDSM 2002-31352, (2002).

[4] Oh, K, "Large eddy simulation of the compressible flow over an open cavity", Journal of the KSPE, Korean Society of propulsion Engineers, Vol.7, No.1, (2003), pp.40-48.

[5] Weber, C., "Development of the implicit method for Navier-Stokes simulations", Ph.D. Thesis, CERFACS. (1998), pp.26-30.

[6] Wilcox, D.C., "Turbulence modeling for CFD", DCW Industries, La Canada, California, (1993).

[7] Germano, M., Piomelli, U., Moin, P., and Cabot, W., "A dynamic sub-grid scale eddy viscosity model", Phys. Fluids A, Vol.3, (1991), pp.1760-1765.

[8] Moin, P., Squires, W., Cabot, W., and Lee, S., "A dynamic sub-grid scale model for compressible turbulence and scalar transport", Phys. Fluids A, Vol.3, (1991), pp.2746-2757.

[9] Lilly, D.K., "A proposed modification of the Germano sub-grid closure method", Phys. Fluids A, Vol.4, (1992), pp.633-635.

[10] Lele, S. K., Compact finite difference schemes with spectral-like resolution , J. Computational Phys., Vol. 103, (1992), pp.16-42.

[11] Boersma, B.J., and Lele, S.K., Large Eddy Simulation of a Mach 0.9 Turbulent Jet , AIAA Paper99-1874, (1999).

[12] Poinsot, T., and Lele, S.K., "Boundary conditions for direct simulation of compressible viscous flows", J. Computational Phys. Vol. 101, (1992), pp. 104 -129.

[13] Freund,J.B., Proposed inflow/outflow boundary conditions for direct computation of aerodynamic sound , AIAA J., Vol.35, (1997), pp. 740-742.

[14] Tam, C.K.W., and Block, P.J.W., "On the tones and pressure oscillations induced by flow over rectangular cavites", J. Fluid Mech., Vol.89, (1978), pp.373-399.